

Pronounced induction of endoplasmic reticulum stress and tumor suppression by surfactant-free poly(lactic-co-glycolic acid) nanoparticles via modulation of the PI3K signaling pathway

Chia-Cheng Hou^{1,6}
Tsung-Lin Tsai^{1,6}
Wen-Pin Su⁶
Hsing-Pang Hsieh⁷
Chen-Sheng Yeh^{4,5}
Dar-Bin Shieh¹⁻⁴
Wu-Chou Su^{1,6}

¹Institute of Basic Medical Sciences, ²Institute of Oral Medicine and Department of Stomatology, ³Advanced Optoelectronic Technology Center, ⁴Center for Micro/Nano Science and Technology, ⁵Department of Chemistry, ⁶Department of Internal Medicine, National Cheng Kung University Hospital, College of Medicine, National Cheng Kung University, Tainan, Taiwan; ⁷Division of Biotechnology and Pharmaceutical Research, NHRI, Miaoli, Taiwan

Correspondence: Wu-Chou Su
Department of Internal Medicine,
National Cheng Kung University Hospital,
College of Medicine, National Cheng
Kung University, Tainan 70101, Taiwan
Tel +886 6 235 3535 ext 3120
Fax +886 6 208 4112
Email sunnysu@mail.ncku.edu.tw

Dar-Bin Shieh
Institute of Oral Medicine and
Department of Stomatology,
National Cheng Kung University Hospital,
College of Medicine, National Cheng
Kung University, Tainan 70101, Taiwan
Tel +886 6 235 3535 ext 5410
Fax +886 6 276 6626
Email dshieh@mail.ncku.edu.tw

Background: LY294002 (LY) is a potent inhibitor of phosphatidylinositol 3-kinases (PI3Ks); however, biological applications of LY are limited by its poor solubility and pharmacokinetic profile. This study aimed at developing LY-loaded surfactant-free poly(lactic-co-glycolic acid) (PLGA) nanoparticles (SF-LY NPs) to improve the therapeutic efficacy of LY.

Materials and methods: Cellular viability was measured by MTT assay. The subcellular distribution of NPs was studied using an ultraviolet-visible spectrophotometer and confocal microscope. The expression of cell-death-associated proteins was determined using Western blotting and the in vivo activity of SF-LY NPs was tested in a xenograft animal model.

Results: SF-LY NPs enhanced the intracellular level of LY, induced sustained suppression of AKT, and induced marked cancer cell death. In addition, SF-LY NPs tended to accumulate in the endoplasmic reticulum (ER) and induce pronounced ER stress. Finally, SF-LY NPs exhibited a prominent antitumor effect in vivo.

Conclusion: The surfactant-free formulation of PLGA is critical to the promising anticancer activity of SF-LY NPs.

Keywords: LY294002, AKT, surfactant-free poly(lactic-co-glycolic acid), endoplasmic reticulum stress

Introduction

Phosphatidylinositol 3-kinases (PI3Ks) are lipid kinases that are activated by growth factors or oncogenes,¹ following which they phosphorylate the 3'-hydroxyl group of membrane phosphatidylinositols. Subsequent activation of the AKT (protein kinase B, PKB) downstream pathway by PI3Ks promotes cell survival.² Aberrations in PI3K signaling commonly occur in many cancers; for example, *PIK3CA*, which encodes the p110 catalytic subunit of PI3K, is probably the most commonly (15%) mutated kinase in all cancers. In contrast, phosphatase and tensin homolog (*PTEN*), which encodes the phosphatase opposing PI3K, is known to be mutationally or post-translationally inactivated in tumors.^{3,4} The activation of PI3K signaling in cancer also occurs via receptor tyrosine kinases (RTKs), AKT, and RAS.⁵ It is believed that the many variations in PI3K signaling present important therapeutic targets for cancer treatment.

LY294002 (LY) is a potent inhibitor of PI3K activity and acts as a competitive and reversible inhibitor for the ATP-binding site of the enzyme.⁶ It has also been demonstrated to have antitumor activity in vitro.⁷⁻¹⁰ Moreover, LY significantly inhibits growth and ascites formation associated with ovarian carcinoma and induces apoptosis

of nasopharyngeal carcinoma cells in animal xenograft models.^{11–13} However, LY has poor solubility in water and poor pharmacokinetics in vivo.¹⁴ Improvement of the physical and pharmacokinetic properties of LY is therefore desirable for therapeutic application.

Nanotechnology is considered to be a feasible approach for targeted drug delivery by minimizing potential side effects.¹⁵ To date, biocompatible nanoparticles (NPs) comprising various materials such as metals, polymers, and nanomagnets have been employed as nanodrug delivery systems to target cancer cells.^{16–19} Among the nanomaterials available for drug delivery, poly(lactic-co-glycolic acid) (PLGA) has been approved by the US Food and Drug Administration for use in humans.²⁰ It has been demonstrated to be an ideal carrier of drug delivery systems owing to its unique properties, including biodegradable hydrolysis to metabolite monomers (lactic and glycolic acids); easy formulation for hydrophobic, poorly soluble drugs; easy surface modification or bioconjugation for targeting; and high biochemical and physicochemical stability.^{21–23}

A previous study reported the use of a surfactant (polyvinyl alcohol; PVA) to formulate LY-loaded, PVA-containing, PLGA NPs (PVA-LY NPs) for improving LY solubility.²⁴ Although PVA-LY NPs could cause cell death resulting from the sustained release of LY inside cells, the conjugates inhibited cell proliferation to a lesser extent compared with free LY.²⁴ A possible explanation is that the residual PVA associated with PLGA prevented cellular uptake of NPs.²⁵ Accordingly, we developed a novel surfactant-free PLGA copolymer^{26,27} to carry LY. We demonstrate that in the absence of surfactant, LY-loaded, surfactant-free NPs (SF-LY NPs) enhanced the incorporation efficacy of NPs, caused sustained inhibition of AKT phosphorylation, targeted LY to the endoplasmic reticulum (ER) lumen, and effectively decreased cancer cell growth in vitro and in vivo.

Material and methods

Cell culture and reagents

The cell lines H460, H157, H1650, and NL20 were obtained from the American Type Culture Collection (ATCC; Manassas, VA, USA). H460, H157, and H1650 cells were cultured in RPMI-1640 containing 10% fetal bovine serum (FBS; Life Technologies, Carlsbad, CA, USA) and the NL20 cells were grown in Ham's F12 medium supplemented with glucose (2.7 g/L), L-glutamine (2 mM), nonessential amino acids (0.1 mM), insulin (0.005 mg/mL), epidermal growth factor (EGF, 10 ng/mL), transferrin (0.001 mg/mL), hydrocortisone (500 ng/mL), and FBS (4%). The parental

PC14PE6 cell line was generously provided by Dr Fidler (MD Anderson Cancer Center, Houston, TX, USA), and its derivative PC14PE6/AS2 (AS2) cell line was subsequently established in our laboratory.²⁸ The AS2 cells were maintained in Minimum Essential Medium Alpha Modification (α -MEM; Life Technologies) supplemented with 10% FBS. Copolymers of PLGA (molecular weight: 35,000–65,000 Da; lactide:glycolide, 50:50) were purchased from Bio Invigor Corporation (Taipei, Taiwan). PVA, 3-[4,5-dimethylthiazol-2-yl]-2, 5-diphenyltetrazolium bromide (MTT), Nile red, 3-methyladenine (3-MA), bafilomycin A1, dimethyl sulfoxide (DMSO), Tris-HCl, NP-40, ethylene diamine tetra-acetic acid (EDTA), sodium dodecyl sulfate (SDS), ethanol, acetone, sodium chloride, disodium hydrogen phosphate, potassium chloride, trifluoroacetic acid (TFA), and dimethyl fumarate (DMF) were purchased from Sigma-Aldrich (St Louis, MO, USA). ER-Tracker™ Green was purchased from Molecular Probes (Life Technologies) and LY was purchased from Biomol (Plymouth, PA, USA). Antibodies were purchased from Cell Signaling Technology (Danvers, MA, USA).

Preparation of PLGA NPs

The method for preparation of surfactant (PVA)-containing PLGA NPs was described previously,²⁴ while the method for preparation of surfactant-free PLGA NPs (SF NPs) was modified from a previous study.²⁶ In brief, to prepare LY or Nile red-loaded PLGA NPs (SF-LY NPs or SF-Nile red NPs), 50 mg of PLGA polymers was dissolved in 5 mL of acetone and 1 mg of LY or Nile red, respectively, was added. Next, an ethanol/H₂O (50/50, % v/v) solution was added dropwise (1 mL/minute) into the PLGA solution using a tubing pump. The solution was stirred at 240 rpm until the mixture was turbid. The suspension was transferred into 20 mL of deionized water and stirred at 300 rpm for 15 minutes. The organic solvent was then removed under reduced pressure for 30 minutes. To prevent PLGA from aggregating, the solution was filtered using 90 mm filter paper. To measure encapsulation capacity, PLGA NPs were collected and dissolved in acetone and the content of LY was determined using an ultraviolet-visible (UV-Vis) spectrometer (Hewlett-Packard Model 8453; Hewlett Packard, Palo Alto, CA, USA) at a wavelength of 300 nm. Encapsulation capacity (%) was determined by comparing the amount of encapsulated LY with the initial LY concentration.

Transmission electron microscopy (TEM) of NPs

Electron micrographs of PLGA NPs were acquired by placing a drop of the sample onto a copper mesh coated with

amorphous carbon film (79725; Ted Pella Inc, Redding, CA, USA) and dried in a vacuum desiccator (Thermo Scientific Nalgene Vacuum Desiccator, EW-06520-05; Thermo Fisher Scientific, Waltham, MA, USA). PLGA NPs were stained with phosphotungstic acid before TEM (CM-200; Philips, Amsterdam, Netherlands) at 80 KV. The mean diameter and morphology of PLGA NP images were recorded.

In vitro PI3K inhibitor release studies

NPs (50 mg) were added directly to a 1.5-mL Eppendorf tube containing 1 mL of phosphate-buffered saline (PBS; 10 mM, pH 7.4) with 0.1 mL of FBS. The supernatant containing LY released from the PLGA NPs was collected after 10 minutes of centrifugation at 13,000 rpm at various time intervals after the addition of NPs. The total amount of LY in NPs (50 mg) was determined by the addition of acetone to dissolve the PLGA NPs and collection of the supernatant for assays. The amount of LY in the supernatant was measured by high-performance liquid chromatography (HPLC; Agilent 1100 series; Agilent Technologies, Santa Clara, CA, USA). The mobile phase consisted of water (0.1% TFA) and methanol (0.1% TFA; 40:60 v/v). The reverse-phase column used was a CC 125/4 Nucleod UR 100-5 C18 (Macherey-Nagel, Düren, Germany). The column temperature was maintained at 25°C. The flow rate was set at 1.0 mL/minute and the detection wavelength was 300 nm. Sample solution was injected in a volume of 10 µL. The release pattern was defined as the ratio of measured to initial amount of LY encapsulated in the NPs.

MTT cytotoxicity assay

Cells were seeded (5×10^3 per well) in a 96-well culture plate and incubated overnight at 37°C in humidified air containing 5% CO₂. Concentration-effect and time-course studies were performed in the presence of free LY, SF NPs, and SF-LY NPs. After the required incubation periods, 20 µL of MTT reagent stock solution (5 mg/mL in PBS) was added to each well and incubated for 4 hours at 37°C. Plates were centrifuged at 1200 rpm for 5 minutes. After the supernatant was discarded, DMSO (200 µL) was added to each well followed by incubation for 5 minutes. The supernatants were transferred into a new enzyme-linked immunosorbent assay (ELISA) plate and absorbance was measured at 490 nm with an ELISA reader (Varioskan; Thermo Fisher Scientific).

Cytochrome c detection

Cells (5×10^6) were trypsinized and resuspended in ice-cold preparation buffer (10 mM Tris-HCl, pH 7.5, containing

300 mM sucrose supplemented with a protease inhibitor cocktail) on ice for 20 minutes. After incubation, cells were homogenized with Dounce homogenizer and centrifuged at 800 g for 10 minutes at 4°C. The resulting supernatant was centrifuged at 8000 g for 20 minutes at 4°C to yield mitochondria-enriched pellet and cytosolic supernatant fractions. These fractions were used to monitor cytochrome c release from mitochondria to cytosol by Western blotting.

Caspase 3/7 and caspase 8 activity assay

Cells (1×10^4) were lysed in caspase assay buffer, mixed gently, and incubated at room temperature for 3 hours according to the Caspase-Glo™ 3/7 Assay or Caspase-Glo™ 8 Assay (Promega Corporation, Fitchburg, WI, USA) protocol. Caspase activity was quantified in a Veritas™ Microplate Luminometer (Promega).

Intracellular LY uptake

Cells (5×10^3 per well) were seeded onto 6 cm dishes and incubated overnight at 37°C in humidified air containing 5% CO₂. Free LY and NPs (SF-LY and PVA-LY) with equal concentrations of LY (50 µM) were added to the medium. Cells were harvested at the indicated time periods for further analyses. For LY detection in the ER organelle, isolation of the ER was performed with a Sigma-Aldrich ER isolation kit (catalog number ER0100 –1 KT) according to the supplier's instructions. The levels of intracellular LY were measured according to a previously published protocol²⁴ with a slight modification. Briefly, lysed cells were lyophilized to remove water before suspension in 100 µL of DMF and shaken for 1 hour to dissolve internalized LY. The samples were then centrifuged at 14,000 rpm for 1 hour to obtain supernatants for LY quantification by measurement of absorbance on a UV-Vis spectrometer at 300 nm against a standard concentration-absorbance curve.

Intracellular localization by confocal laser microscopy

Viable cells (1×10^5) were plated onto 3.5 cm dishes with 3 mL of culture medium. After overnight incubation, cells were treated with free Nile red or PLGA NPs loaded with Nile red (SF-Nile red NPs) for 3 hours of incubation and stained with ER tracker™ Green dye according to the manufacturer's protocol (Molecular Probes®; Life Technologies) and 4',6-diamidino-2-phenylindole (DAPI). After replacement of original medium with particle-free, fresh medium, cells were immediately imaged with a scanning confocal microscope (Fluoview® FV-1000; Olympus Corporation, Tokyo, Japan)

set to detect fluorophores by A laser (excitation 405, 488, or 546 nm).

Western blot analysis

Cells were lysed on ice for 30 minutes with whole-cell extract lysis buffer (50 mM Tris-HCl, pH, 7.2–7.8; 1% NP-40; 2 mM EDTA; 100 mM NaCl; 0.1% SDS supplemented with protease inhibitor cocktail; Roche Applied Sciences, Indianapolis, IN, USA). Lysates were collected by centrifugation at 14,000 rpm for 10 minutes and protein concentration was determined by the Bradford assay (Bio-Rad Laboratories, Hercules, CA, USA). Protein extracts (20–50 µg) were boiled for 5 minutes in sample buffer before separation by sodium dodecyl sulfate polyacrylamide gel electrophoresis (SDS-PAGE). The proteins were transferred to polyvinylidene fluoride (PVDF) membranes (Millipore, Billerica, MA, USA) at 400 mA for 1.5 hours using an electroblotter (Amersham Pharmacia Biotech Inc, Piscataway, NJ, USA). Membranes were blocked with a mixture of Tris-buffered saline and Tween 20 (TBST) containing 5% nonfat milk for 1 hour at room temperature and incubated overnight at 4°C with pAKT-S473, AKT, CHOP, p-JNK, JNK, GRP78, and actin antibodies. Proteins were detected with horseradish peroxidase-conjugated secondary antibodies using an enhanced chemiluminescence (ECL) kit (Amersham) according to the manufacturer's instructions.

Design and transfection of small interfering RNA (siRNA)

The 21-nucleotide CHOP siRNA, 19-nucleotide JNK siRNA, and negative control duplexes were purchased from Dharmacon Research (Thermo Fisher Scientific). The CHOP siRNA sequence used was 5'-AAGAACCAGCAGAGGUCACAA-3' and the siRNA JNK sequence for targeting both JNK isoforms (JNK1 and JNK2) was 5'-GAAAGAATGTCCTACCTTC-3'. The transfection of siRNA oligonucleotides was performed with LipofectAMINE 2000 (Life Technologies) according to the manufacturer's recommendations. In brief, 16 µL of LipofectAMINE 2000 reagent was mixed with 400 µL of Opti-MEM (Life Technologies) at room temperature for 5 minutes and incubated with a mixture of 12 µL of siRNA duplex and 400 µL of Opti-MEM for an additional 20 minutes at room temperature. The complexes were then applied to cultured cells at 70% confluence on a 60 mm plate. After incubating for 6 hours, the medium was replaced with fresh medium supplemented with 10% FBS and 1% penicillin/streptomycin.

Tumor xenograft experiments

Female athymic nude mice (6–8 weeks) were obtained from the National Laboratory Animal Center in Taiwan. All animal studies were approved by the Animal Welfare Committee at National Cheng Kung University for the same environment with controlled temperature, humidity, and a 12-hour light/dark cycle. Mice were subcutaneously inoculated in the flank with PC14PE6/AS2 cells (1×10^6 cells/mouse in 100 µL of PBS) and randomized at approximately 14 days after implantation, when the tumor size reached 50–60 mm³. The following intratumoral injections were administered every other day for a total of six times to the xenograft mice: normal saline (n = 8), SF NPs only (n = 8), LY (1 mg/kg; n = 8), or SF-LY NPs (LY, 1 mg/kg; n = 10). The treated mice were monitored for signs of distress and tumor size was measured with calipers. Tumor volume was calculated according to the following formula: (volume = long axis × short axis² × 0.5). For ethical reasons, mice were sacrificed when tumor size reached 4000 mm³.

Statistical analysis

All experiments were repeated at least three times. The data are presented as means ± standard error of the mean. Statistical analyses were performed using one-way and two-way analysis of variance (ANOVA). Differences in the mean values for apoptosis, tumor growth, and body weight response to treatment were compared between groups using two-way ANOVA with Bonferroni post-testing. All other data for statistical differences between experimental groups were analyzed using one-way ANOVA. A *P*-value of < 0.05 was considered statistically significant.

Results

Characteristics of surfactant-free PLGA NPs

The particle size and polydispersity index (PDI) of SF NPs and SF-LY NPs were analyzed by dynamic light scattering (DLS; Table 1). The mean diameter of SF NPs was 74.5 ± 1.74 nm, while that of SF-LY NPs was 98.9 ± 2.64 nm. Representative transmission electron micrographs illustrate that SF-LY NPs were spherical in shape and monodispersed. The mean diameter of SF-LY NPs was 80 nm as measured by TEM (Figure 1A). The encapsulation efficiency and loading capacity of LY in SF NPs was 37% and 7.4 µg/mg, respectively. The release of LY from the SF-LY NPs was measured in vitro in serum-containing PBS. After incubation, there was a burst of initial release of LY (approximately 27% of total loaded LY) within the first 6 hours, followed by a slow release of LY (57% of the total LY amount) from 6 to

Table I Particle size, polydispersity index (PDI), entrapment efficiency, and drug-loading capacity of SF NPs and SF-LY NPs as detected by dynamic light scattering (DLS)

	Particle size (nm) ^a	Polydispersity index	Encapsulation efficiency (%) ^b	Loading capacity (µg/mg)
SF NPs	74.5 ± 1.74	0.19 ± 0.01	N/A	N/A
SF-LY NPs	98.9 ± 2.64	0.134 ± 0.03	37% ± 2.1%	7.4 ± 0.42

Notes: ^aData represent mean ± SEM from three independent experiments; ^befficiency expressed as a percentage mean of three determinations ± standard deviation of drugs recovered in NPs compared with theoretical drugs loaded in the generated formulations.

Abbreviations: LY, LY294002; N/A, not applicable; NPs, nanoparticles; SEM, standard error of the mean; SF NPs, surfactant-free NPs; SF-LY NPs, surfactant-free NPs loaded with LY.

12 hours and a sustained release of approximately 73% of the total loaded LY over the next 7 days (Figure 1B).

In vitro cytotoxicity assay

To evaluate the dose-dependent cytotoxicity of SF NPs, free LY, PVA-LY NPs, and SF-LY, we conducted MTT assays

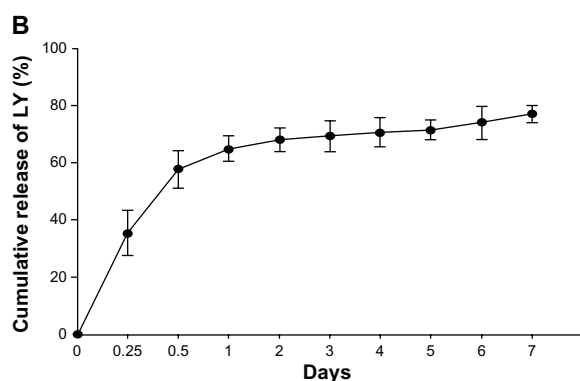
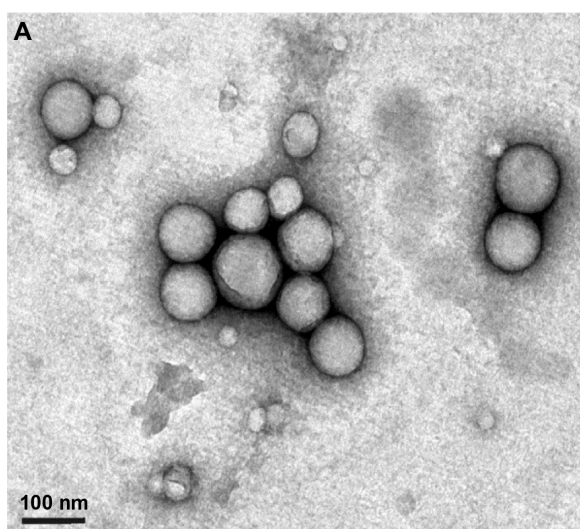


Figure 1 Characterization of SF-LY NPs

Notes: (A) The analysis of SF-LY NP morphology by TEM. (B) Drugs released from SF-LY NP nanoparticles at the indicated time points were measured by UV-VIS spectrometry at a wavelength of 300 nm. Data represent mean ± SEM from three independent experiments.

Abbreviations: LY, LY294002; NPs, nanoparticles; SEM, standard error of the mean; SF-LY NPs, surfactant-free NPs loaded with LY; TEM, transmission electron microscopy; UV-VIS, ultraviolet-visible.

in AS2 (*PTEN*-null), H157 (*PIK3CA* mutation, *PTEN*-null), H460 (*PIK3CA* mutation), and H1650 (EGFRΔE747-A750 mutation, *PTEN*-null) cells (Figure 2A). No suppression of cell growth was evident after AS2, H460, and H157 cells were treated with SF NPs and PVA-LY NPs for 48 hours or after H1650 cells were treated with SF NPs and PVA-LY NPs for 24 hours. Treatment with free LY induced modest cytotoxicity in all four cell lines, whereas treatment with a low concentration of LY (0.25–1.00 µM) in SF-LY NPs induced marked cellular death in the H460, H157, and H1650 cell lines. A relatively high concentration of LY (5 µM) was required in SF-LY NPs to induce similar cytotoxicity in AS2 cells. A time-course study of cytotoxicity was conducted with a fixed concentration of LY compounds (Figure 2B). Treatment with SF-LY NPs again resulted in a significantly greater suppression of cell growth in these lung cancer cell lines compared with treatment with free LY and PVA-LY NPs. The half maximal inhibitory concentration (IC_{50}) value for free LY in the four cancer cell lines was 25–50 µM; however, the IC_{50} values for PVA-LY NPs in the four cell lines were greater than 50 µM (Figure 2C). These results are consistent with an earlier report²⁴ that PVA-LY NPs are less effective than free LY in the inhibition of cancer cell growth. Taken together, these findings suggest that the cytotoxicity of SF-LY NPs is greater than that of PVA-LY NPs and free LY and that a relatively low concentration of LY in SF-LY NPs is sufficient to induce cancer cell death. Next, we examined the cytotoxicity of SF-LY NPs on an NL20 cell line; an immortalized, nontumorigenic, human, bronchial epithelial cell line, in a dose-dependent manner (Figure 2D). Even after treatment with SF-LY NPs containing relatively high concentrations of LY (0.25 to 5 µM), the growth suppression rate was approximately 15%. The toxicities from SF NPs, free LY, PVA-LY NPs, and SF-LY NPs to NL20 cells were comparable. The data show that there is only modest toxicity of SF-LY NPs to NL-20 cells, suggesting that the therapeutic window of SF-LY NPs is promising.

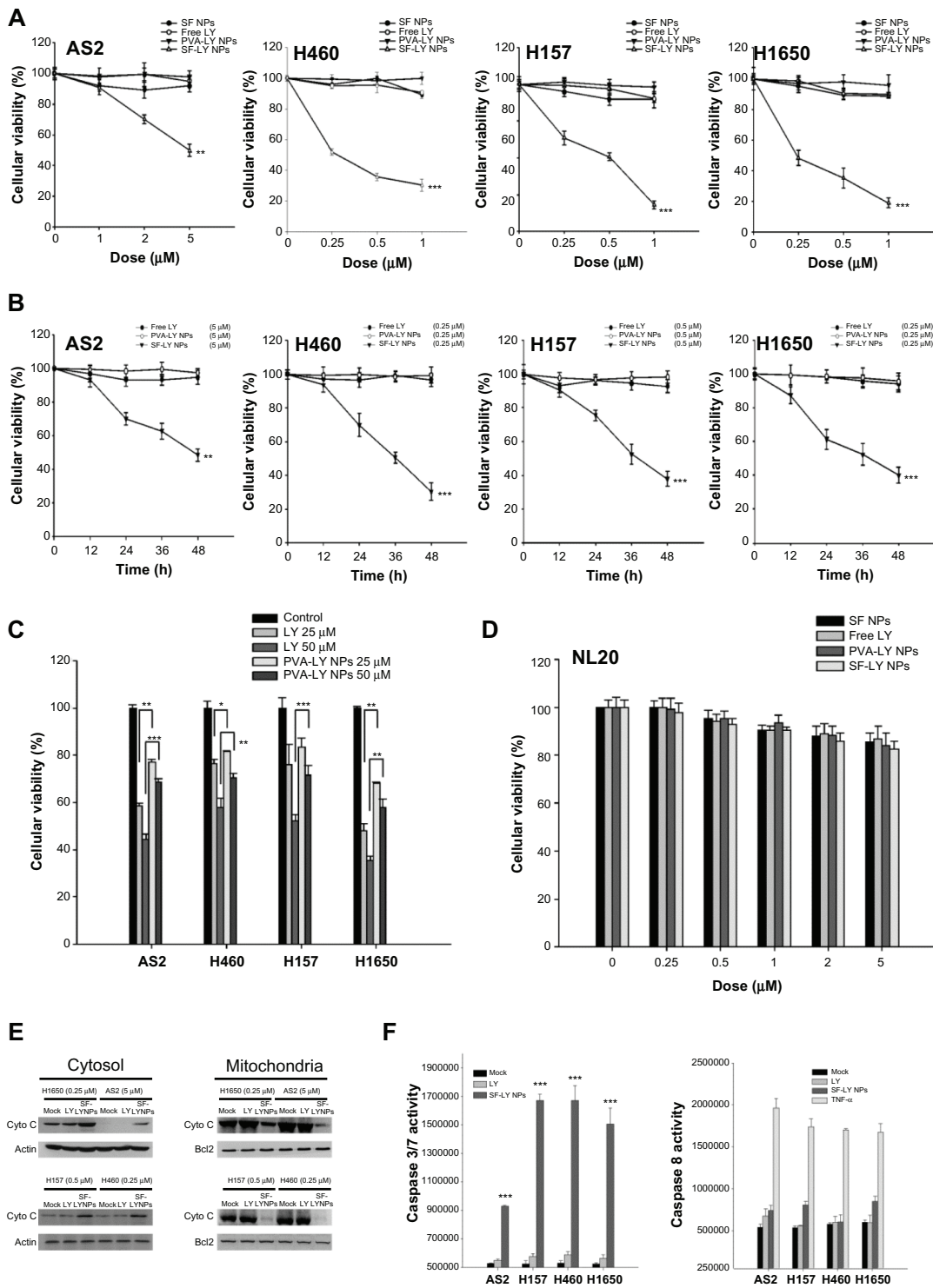


Figure 2 Cytotoxic effects of SF-LY NPs determined by MTT assay.

Notes: (A) The concentration-dependent effect on viability of four lung cancer cell lines. (B) Time-course study of cytotoxicity by MTT assay following treatment with LY or SF-LY NPs. (C) The analysis of cytotoxicity by MTT assay following treatment with LY or PVA-LY NPs. (D) The effect on viability of normal lung cells (NL20) by MTT assay following treatment with LY or PVA-LY NPs. (E) Cytochrome c was monitored by Western blotting after treatment with free LY and SF-LY NPs. (F) Caspase 3/7 or caspase 8 activity was detected after treatment with free LY and SF-LY NPs. The concentrations of free LY and SF-LY NPs were 5 μM for the AS2 cell line, 0.5 μM for the H157 cell line, and 0.25 μM for the H460 and H1650 cell lines. The concentration of TNF-α was 50 ng/mL. Each experiment was repeated three times. Data are expressed as mean ± SEM. *P < 0.05; **P < 0.005; ***P < 0.001 (free LY versus SF-LY NPs). TNF-α is positive control for caspase 8-dependent cell death.

Abbreviations: cyto c, cytochrome c; LY, LY294002; MTT, 3-[4,5-dimethylthiazol-2-yl]-2, 5-diphenyltetrazolium bromide; NPs, nanoparticles; PVA, polyvinyl alcohol; PVA-LY NPs, PVA NPs loaded with LY; SEM, standard error of the mean; SF NPs, surfactant-free NPs; SF-LY NPs, surfactant-free NPs loaded with LY; TNF-α, tumor necrosis factor alpha.

The mechanisms of cell death induced by SF-LY NPs

First, we analyzed the mechanism of cell death²⁹ induced by SF-LY NPs using flow cytometric analysis (annexin V/propidium iodide [PI] double staining method) and found that SF-LY NPs, but not free LY, induced significant cellular apoptosis in the four cell lines (Figure S1). The phenomenon of apoptosis was further supported by DAPI staining, which showed an increase in chromatin condensation in SF-LY NP-treated cells (Figure S2). We next examined the release of cytochrome c from mitochondria into the cytosol. Treatment with SF-LY NPs resulted in higher levels of cytosolic cytochrome c in four lung cancer cells compared with free LY (Figure 2E). To further characterize the type of apoptosis activated, we measured the activities of caspase 3/7 and caspase 8 using a luminescent assay kit (Figure 2F). Although SF-LY NPs induced significantly high caspase 3/7 activities, they had little effect on caspase 8 activities in the four cells (Figure 2F). With regard to the free LY, it only modestly induced both caspase 3/7 and 8 activities in the four cells. We conclude that SF-LY NP-induced cell death occurs primarily via the intrinsic apoptotic pathway.

The effects of SF-LY NPs on phosphorylation of AKT in cells

The phosphorylation of serine 473 on AKT in response to different concentrations of LY, PVA-LY NPs, or SF-LY NPs was measured in AS2, H157, H460, and H1650 cell lines by Western blotting (Figure 3A). The ratio of pAKT/AKT was calculated for comparison of the effects of the test agent effects on the cells (Figure 3A). At the indicated concentrations, only SF-LY NPs effectively suppressed the levels of constitutively phosphorylated AKT in the four cancer cell lines. A sustained (>24 hours) suppression of AKT phosphorylation was observed in H460, H157, and H1650 cells in response to a fixed concentration of SF-LY NPs. The same concentration of free LY had no effect (Figure 3B). In AS2 cells, free LY at a concentration of 5 μ M induced a transient suppression of AKT phosphorylation at 8 hours, whereas the suppression of AKT phosphorylation by SF-LY NPs began after 8 hours and lasted up to 48 hours. In contrast to free LY, PVA-LY NPs with 25 μ M LY were effective in decreasing AKT phosphorylation only in H1650 cells (Figure 3C). The difference between the phosphorylation levels in the four cell lines suggested that refractoriness to PVA-LY NPs is independent of the activation status of the target protein.²⁴ Therefore, SF-LY NPs, but not free LY or

PVA-LY NPs, can induce sustained suppression of AKT phosphorylation with relatively low concentrations of LY in cancer cells.

Internalization and subcellular accumulation of NPs

Analysis of the intracellular levels of LY in these lung cancer cell lines after exposure to equivalent concentrations of free LY, SF-LY NPs, or PVA-LY NPs for various time periods (Figure 4A) revealed that the intracellular LY levels of cells were saturated within 8 hours and declined gradually thereafter in response to free LY, SF-LY NPs, and PVA-LY NPs. The intracellular LY levels were highest in cells treated with SF-LY NPs, whereas the intracellular levels of LY after treatment with PVA-LY NPs were similar to those of free LY following incubation for the same time intervals, confirming the results of the previous report²⁴ that the intracellular LY concentration in LY-loaded PLGA NPs with PVA was similar to that in free LY. Therefore, our results showed that intracellular effects are greatly enhanced when induced by SF NPs in all lung cancer cell lines. Next, the subcellular localization of SF NPs was studied using confocal microscopy. Nuclei stained with DAPI (blue) were observed by confocal microscopy, and the ER, marked by ER tracker in green, was disturbed in the perinuclear region. Following treatment with native Nile red or SF-Nile red NPs for 3 hours, Nile red carried by SF NPs tended to colocalize with ER (yellow spot). This colocalization was not observed when cells were treated with native Nile red (Figure 4B) or PVA-Nile red NPs (Figure S3), where the Nile red staining is separated from green staining. The data suggest that SF-Nile red NPs target Nile red to ER. To provide more evidence to show the colocalization, we isolated the ER organelle from the cytosol and separately measured the concentration of LY in ER and cytosol after treatment with free LY or SF-LY NPs in the four cell lines. The amount of LY in the ER was significantly higher after SF-LY NP treatment than after free LY treatment (Figure 4C).

SF-LY NPs induced ER stress and ER stress-related apoptosis in cancer cells

Following the observation that SF NPs may target their payloads to ER, we investigated whether ER stress could be induced by SF-LY NPs. We assayed the expression of three important ER stress markers: CHOP, phosphorylated JNK, and GRP78. In H460, H157, and H1650 cells, the SF-LY NP-induced elevation of CHOP and GRP78 began at 3 hours

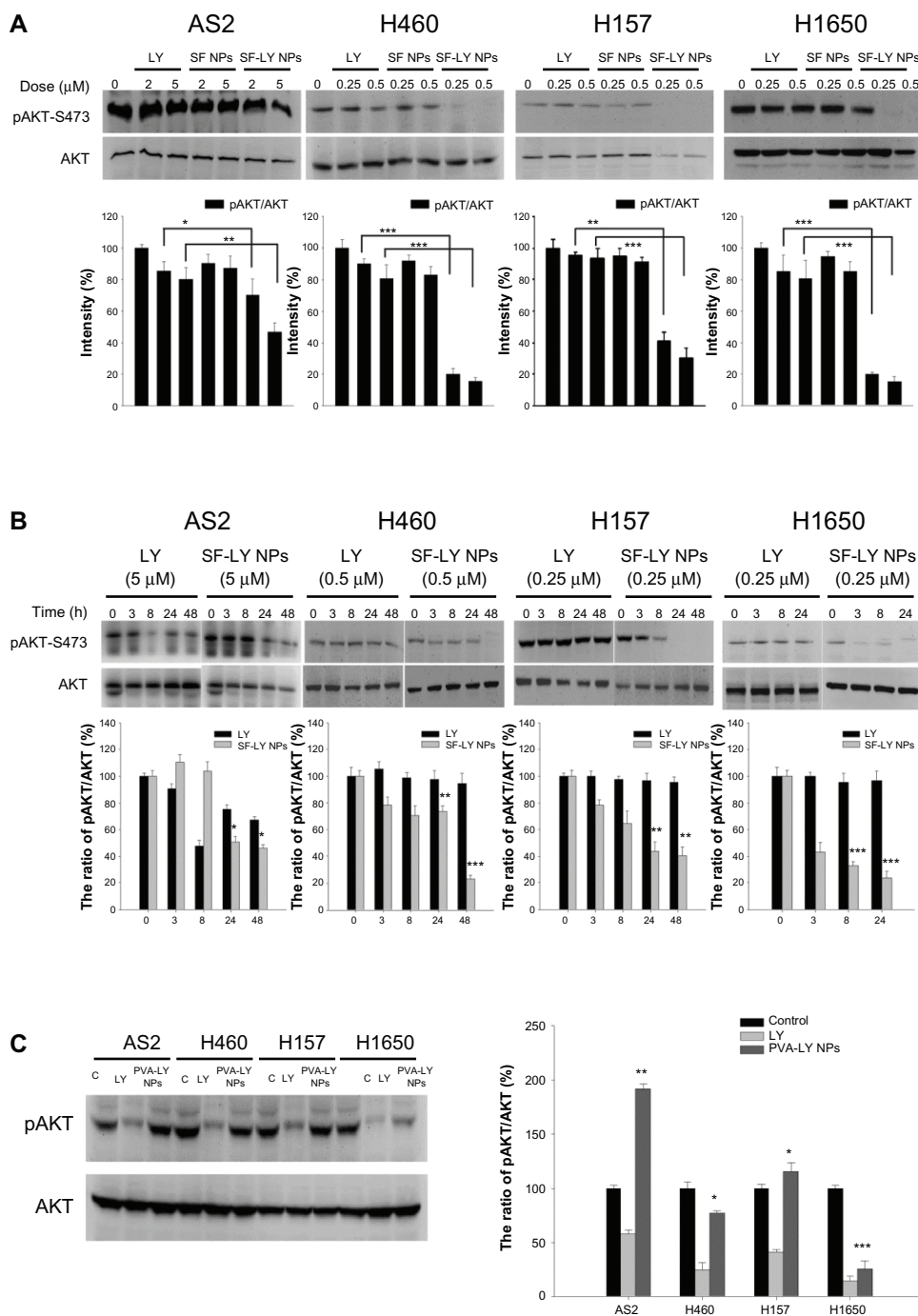


Figure 3 The level of activated AKT by SF-LY NPs.

Notes: Western blots showing levels of phosphorylated AKT in four cell lines following treatment with LY or SF-LY NPs. (A) A concentration-dependent effect and (B) a time-course study. (C) Phosphorylated AKT in response to treatment with LY or PVA-LY NPs. Density detection by ImageJ software. Data represent mean ± SEM from three independent experiments. **P* < 0.05; ***P* < 0.005; ****P* < 0.001 (free LY versus SF-LY NPs).

Abbreviations: LY, LY294002; PVA, polyvinyl alcohol; PVA-LY NPs, PVA NPs loaded with LY; NPs, nanoparticles; SEM, standard error of the mean; SF NPs, surfactant-free NPs; SF-LY NPs, surfactant-free NPs loaded with LY; pAKT, phosphorylated AKT.

and persisted up to 24 hours, whereas the CHOP and GRP78 expression induced in AS2 cells began 24–48 hours after treatment with SF-LY NPs (Figure 5A). The levels of phosphorylated JNK increased rapidly within 3 hours in H157, H460, and H1650 cells after SF-LY NP treatment, whereas

the elevation of phosphorylated JNK occurred 24 hours after SF-LY NP treatment in the AS2 cell line. In the four cell lines, treatment with free LY at a dose equivalent to that in SF-LY NPs had very little effect on the expression of CHOP, GRP78, and phosphorylated JNK (Figure 5A). Treatment with

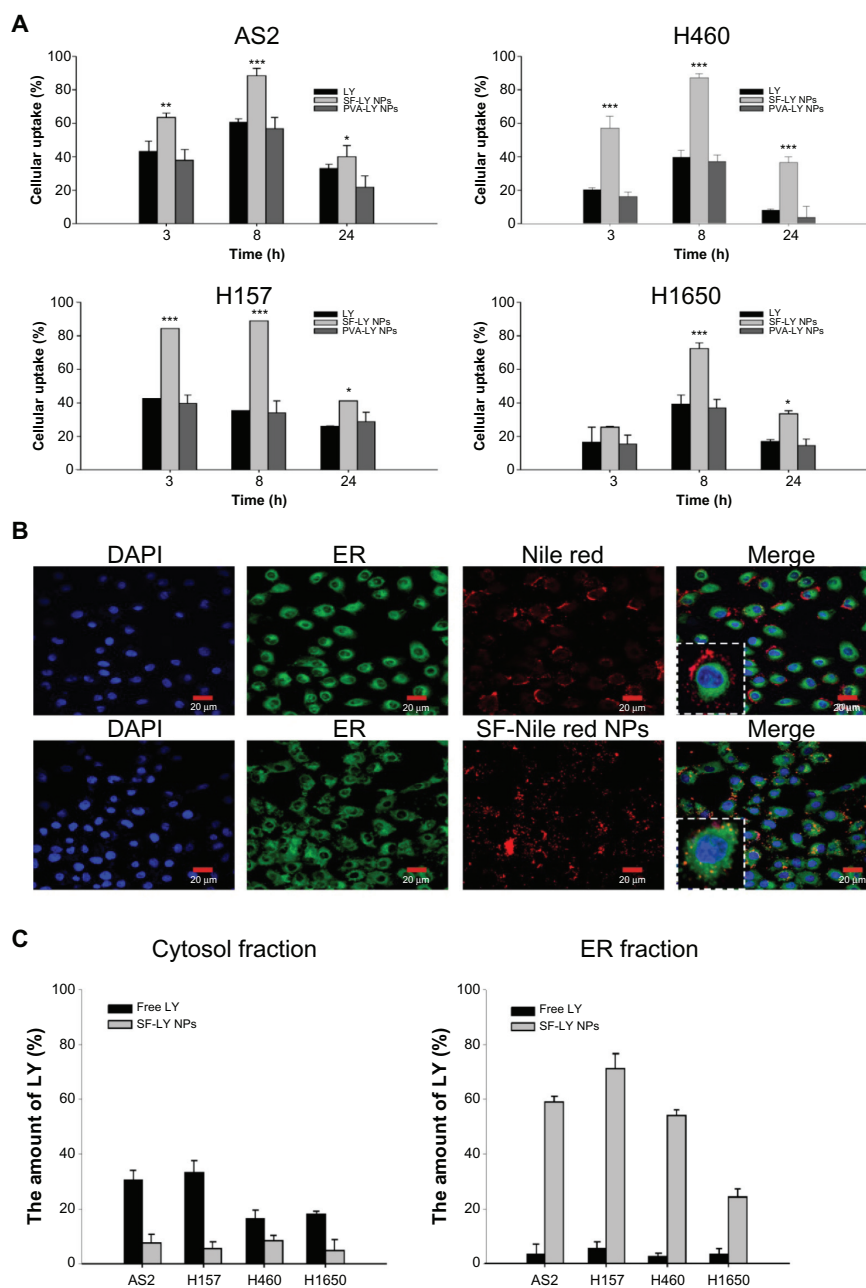


Figure 4 Levels of intracellular incorporation and intracellular localization of PLGA NPs in lung cancer cell lines.

Notes: (A) Graphs show intracellular levels of LY after exposure to LY, SF-LY NPs, or PVA-LY NPs, with an equivalent concentration of LY (50 μ M) for the indicated time points in the four cell lines. Data represent mean \pm SEM from at least three independent experiments. * $P < 0.05$; ** $P < 0.005$; *** $P < 0.001$ (free LY versus SF-LY NPs). (B) Confocal microscopic analysis of native Nile red and SF-Nile red NPs. The cells were incubated with native Nile red or SF-Nile red NPs for 3 hours at 37°C, stained with ER tracker and DAPI, extensively washed, and imaged for living cells under a confocal microscope. Magnified cells in the left lower square show the difference in cellular localization between native Nile red and SF-Nile red NPs (blue: DAPI-stained nucleus; green: ER tracker dye; red: native Nile red or SF-Nile red NPs). (C) Graphs show the levels of LY after exposure to free LY or SF-LY NPs with an equivalent concentration of LY (50 μ M) in subcellular fraction.

Abbreviations: ER, endoplasmic reticulum; DAPI, 4',6-diamidino-2-phenylindole; LY, LY294002; NPs, nanoparticles; PLGA, poly(lactic-co-glycolic acid); PVA, polyvinyl alcohol; PVA-LY NPs, PVA-NPs loaded with LY; SEM, standard error of the mean; SF NPs, surfactant-free NPs; SF-LY NPs, surfactant-free NPs loaded with LY; SF-Nile red NPs, surfactant-free NPs loaded with Nile red.

SF NPs alone did not induce expression of CHOP (Figure S4). These findings suggest that SF-LY NPs, but not free LY or SF NPs, can induce ER stress. Because CHOP has been implicated in ER stress-induced cell death³⁰ and the activation of JNK by unfolding protein response (UPR) may lead to

apoptotic cell death,³¹ we investigated whether SF-LY NP-induced ER stress contributed to apoptotic death. We used salubrinal to block ER stress and SP600125 to inhibit JNK function in the four cancer cell lines and observed that pretreatment with salubrinal or SP600125 alone slightly rescued

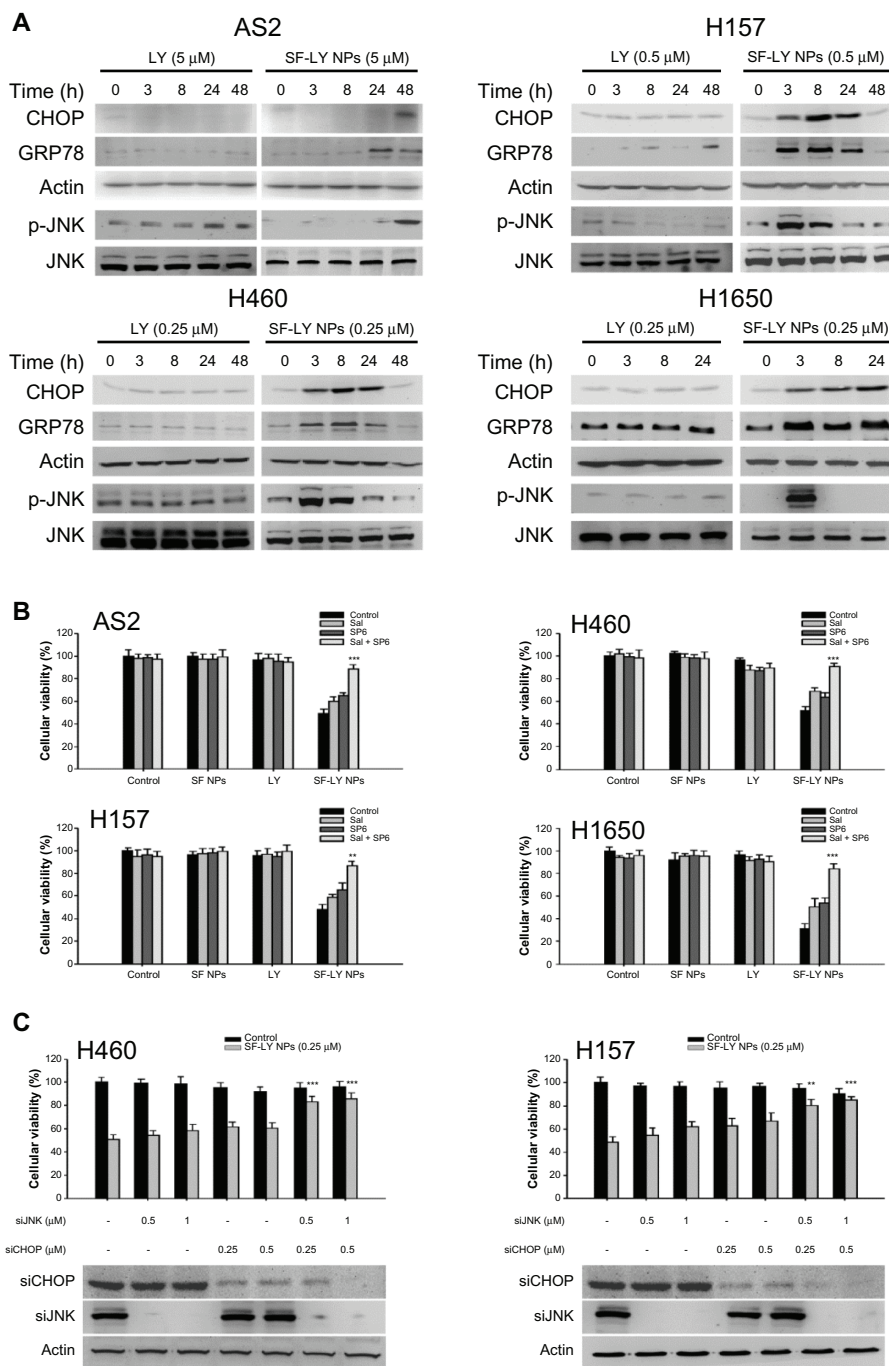


Figure 5 The regulation of ER status after treatment with free LY or SF-LY NPs.

Notes: (A) The change in CHOP, activated JNK expression, and GRP78 status after treatment with free LY or SF-LY NPs in four lung cancer cell lines. (B) Analysis of cytotoxicity by MTT assay after treatment with salubrinal, SP600125, or both. Each experiment was repeated three times. Data are mean \pm SEM. $**P < 0.005$; $***P < 0.001$. (C) Analysis of cytotoxicity by MTT assay and immunoblotting after siRNA treatment for CHOP, JNK, or both. Data are mean \pm SEM from three independent experiments. $**P < 0.005$; $***P < 0.001$.

Abbreviations: ER, endoplasmic reticulum; LY, LY294002; MTT, 3-[4,5-dimethylthiazol-2-yl]-2, 5-diphenyltetrazolium bromide; NPs, nanoparticles; sal, salubrinal; SEM, standard error of the mean; SF NPs, surfactant-free NPs; SF-LY NPs, surfactant-free NPs loaded with LY; SP, SP600125.

SF-LY-NP-induced cell death in the four cell lines. Again, the combination of salubrinal and SP600125 significantly rescued cell death induced by SF-LY NPs (Figure 5B). The data suggested that both JNK and CHOP are critical, but redundant, in mediating cell death induced by SF-LY NPs

via ER stress. We attempted to silence endogenous CHOP expression using siRNA. After transfection of the siRNA into the four cell lines, CHOP expression was suppressed in H460 and H157 cells, but not in the AS2 and H1650 cells. Accordingly, we selected H460 and H157 for further studies.

We treated the two cell lines with free LY or SF-LY NPs after silencing CHOP or JNK with siRNA. The silencing of CHOP or JNK alone partially abolished the antiproliferative activity of SF-LY NPs, whereas the combination of CHOP and JNK siRNA to silence both proteins together restored cell death induced by SF-LY NPs (Figure 5C). ER stress in cells was reported to induce autophagy.³² It is intriguing to ask whether SF-LY NP treatment induces autophagy in cancer cells. We found that the LC3 protein converted from Type I to Type II, a hallmark of autophagy, in cells treated with SF-LY NPs but not free LY (Figure S5A). We used autophagy inhibitors, including 3-MA (inhibition of autophagosome formation) and bafilomycin A1 (inhibition of autophagosome and lysosome fusion), to characterize the impact of SF-LY NP-induced autophagy on cell viability. Pretreatment with 3-MA or bafilomycin A1 further enhanced cell death induced by SF-LY NPs (Figure S5B), indicating that the activation of autophagy by SF-LY NP treatment is essential for cell survival.

In vivo efficacy in an AS2 xenograft mouse model

To investigate whether LY in the SF NP formulation was active in vivo, we injected it intratumorally into mice bearing tumor xenografts. A previous study suggested that localized drug delivery through intratumoral administration is an attractive approach, given that direct application permits higher concentrations of the drug to access the tumor tissue and avoid entering the systemic circulation.³³ An AS2 tumor model was developed in athymic mice. After the average tumor volume reached 50–60 mm³ (approximately 14 days), the following regimens were administered by intratumoral injections every other day for a total of six times: (1) saline, (2) LY (1 mg/kg), (3) SF NPs (1 mg/kg), and (4) SF-LY NPs (1 mg/kg). The change in tumor volume from the initial volume (50–60 mm³) was monitored until the average tumor size reached 3000–4000 mm³ after intratumoral injection. The results showed that tumor volume steadily increased with time in mice injected with saline, SF NPs, and free LY, reaching an approximately 40-fold increase from the size of the original tumor after 12–14 days. In contrast, administration of SF-LY NPs (1 mg/kg) effectively slowed tumor growth, restricting the total increase in tumor volume to approximately 2.5–3 times the original tumor size (Figure 6A). No significant difference in body weight was observed within or among each group of mice (Figure 6B), indicating that SF NPs, free LY, and SF-LY NPs were not toxic to mice. Collectively, these results indicated that

intratumoral injection of SF-LY NPs induced long-lasting inhibition of tumor growth.

Discussion

In this study, we formulated a surfactant-free PLGA copolymer^{26,27} as a carrier for LY and demonstrated that in the absence of surfactant, SF-LY NPs could enhance the incorporation efficacy of NPs, cause sustained inhibition of AKT phosphorylation, target LY to the ER lumen, and effectively decrease cancer cell growth in vitro and in vivo.

The size (diameter) of SF-LY NPs was in the range of 80–100 nm. NPs of this size have the potential to avoid retention in the reticuloendothelial system (RES).³⁴ In a previous study, we found that surfactant-free PLGA copolymers could be easily and directly conjugated on their surface.²⁶ This advantage was particular to surfactant-free, but not surfactant-containing, PLGA NPs.²⁶ Because the hydrophilicity of surfactant PVA may decrease intracellular uptake and lysosomal escape of NPs,^{25,35,36} we attempted to formulate PVA-LY NPs and examine their activities in the four cell lines (Figure 2C). Similar to the findings in a previous study,²⁴ PVA-LY NPs showed inferior antiproliferative activity compared with SF-LY NPs. According to the release profile of SF-LY NPs, LY is released from NPs in a sustained manner. The results of in vitro experiments showed a sustained inhibition of AKT phosphorylation for up to 48 hours in cells treated with SF-LY NPs, but not in cells treated with free LY (Figure 3). The sustained inhibition of AKT activity by SF-LY NPs may contribute substantially to its prominent proapoptotic property, given that constitutive activation of AKT may promote cellular survival in lung cancer cells.³⁷ Among the four cell lines incubated with SF-LY NPs, the ratio of LY uptake in AS2 cells was the lowest (Figure 4A). The effect of suppressing AKT phosphorylation by SF-LY NPs in AS2 cells was also inferior to that observed in the other three lung cancer cell lines. Consequently, SF-LY NPs induced less cell death in the AS2 cell line than in the other cell lines. Therefore, the ratio of cellular uptake of NPs may influence the final therapeutic effects. Our data demonstrated that cells take up a greater amount of NPs synthesized without surfactant compared with surfactant-containing NPs. The higher intracellular concentration of LY delivered by SF-LY NPs contributed to the greater cytotoxicity of SF-LY NPs compared with that of free LY and PVA-LY NPs in cancer cells.

The four cancer cell lines used in this study harbor genetic alterations in the PI3K pathway. Both AS2 and H1650 cells are *PTEN*-null, whereas H460 cells harbor a

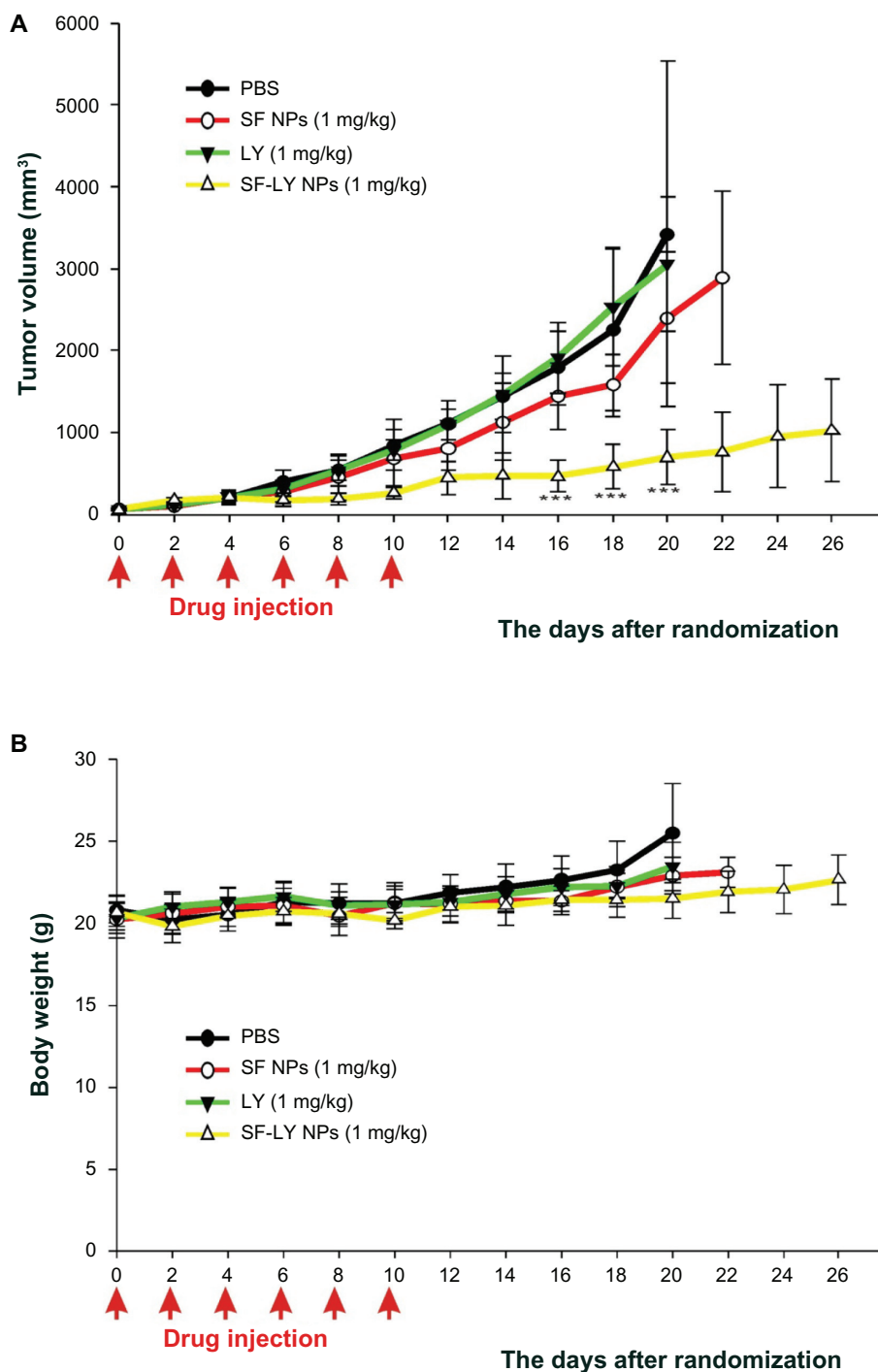


Figure 6 The effect of intratumoral injection in vivo.

Notes: (A) The change in tumor volume was monitored for 14 days after injection of saline (black), PLGA only (1 mg/kg; red), free LY (1 mg/kg; green), or SF-LY NPs (1 mg/kg; yellow) into tumor-bearing mice. ****P* < 0.001 (free LY versus SF-LY NP group at 16, 18, and 20 days). (B) Body weights for each group were determined every 2 days.

Abbreviations: LY, LY294002; NPs, nanoparticles; PBS, phosphate-buffered saline; PLGA, poly(lactic-co-glycolic acid); SF NPs, surfactant-free NPs; SF-LY NPs, surfactant-free NPs loaded with LY.

PIK3CA mutation and H157 cells are *PTEN*-null and harbor a mutation in PIK3CA. Although a low concentration of free LY induced modest cellular death in the four cell lines, treatment with SF-LY NPs over the same concentration range resulted in significantly increased cellular death. In contrast,

in a normal bronchial cell line called NL-20, we found only modest toxicity of SF-LY NPs to NL-20 cells. Toxicities of SF NPs, free LY, PVA-LY NPs, and SF-LY NPs to normal cells are comparable, suggesting that SF-LY NPs offer a promising therapeutic window for cancer therapy.

A study of the subcellular localization of SF NPs revealed that SF NPs targeted Nile red to the perinuclear region and colocalized with an ER marker (Figure 4B). A previous study reported that PLGA NPs could localize with specific organelles such as ER and the Golgi apparatus,³⁸ suggesting that SF NPs in this study delivered their payloads to ER and induced specific cellular responses. We examined the changes in ER stress-related proteins and found that treatment with SF-LY NPs, but not free LY or SF NPs, enhanced the expression of CHOP, phosphorylated JNK, and GRP78 in the four lung cancer cell lines (Figure 5A and Figure S4). We further demonstrated that the induced ER stress facilitates cellular apoptosis. The inhibition of CHOP or JNK alone by either siRNA or inhibitors partially abolished the antiproliferative activity of SF-LY NPs, whereas combinational inhibition of CHOP and JNK significantly rescued the cell death induced by SF-LY NPs (Figure 5B and C). The data suggested that both JNK and CHOP are critical but redundant in mediating cell death induced by SF-LY NPs via ER stress. Interestingly, the induction of ER stress signals by SF-LY NPs is less obvious in AS2 cells than in the other three cell lines. These observations are consistent with those for SF-LY NPs, which produce the least cytotoxic effects on AS2 cells.

Although SF-LY NPs induced significantly high caspase 3/7 activities, they exerted little effect on caspase 8 activities in the four cancer cell lines (Figure 2F). Free LY only modestly induced both caspase 3/7 and 8 activities in the four cell lines. We conclude that SF-LY NP-induced cell death is primarily through the intrinsic apoptotic pathway. We found that after SF-LY NP treatment, autophagy was induced in the four cancer cell lines (Figure S5A). Because treatment with autophagy inhibitors 3-MA and bafilomycin A1 further enhanced cell death induced by SF-LY NPs (Figure S5B), we considered the activation of autophagy by SF-LY NPs treatment to have protective effects on cell survival.

Although the AS2 cells are relatively insensitive to treatment with SF-LY NPs in vitro (Figure 2), they exhibit rapid xenograft tumor growth in nude mice. For this reason, the AS2 xenograft model was chosen to test the in vivo antitumor activity of SF-LY NPs. Treatment with SF-LY NPs significantly suppressed growth of AS2 xenograft tumors in mice, suggesting that they have strong in vivo antiproliferative activities (Figure 6), even against tumors generated from a less sensitive cell line.

Conclusion

We successfully synthesized SF-LY NPs and demonstrated their potential application in biomedical engineering.

The particle size, encapsulation efficiency, and the controlled release kinetics of SF NPs were particularly suited for drug delivery. It was demonstrated that SF-LY NPs induced significantly increased cell death through the apoptotic pathway in lung cancer cells compared with free LY and PVA-LY NPs. Moreover, surfactant-free PLGA NPs were able to enhance intracellular uptake of LY and subsequently deliver their payloads to ER, inducing ER stress. Finally, we demonstrated that SF-LY NPs have impressive in vivo antitumor activities. We conclude that surfactant-free PLGA is an ideal nanocarrier for the LY compound.

Acknowledgments

This research was supported in part by the Ministry of Education, Taiwan, ROC, and the Aim for the Top University Project to the National Cheng Kung University (NCKU). The authors also thank the Department of Health and National Science Council of Taiwan for financial support of this research under contracts DOH99-TD-B-111-002, DOH99-TD-C-111-003, DOH100-TD-PB-111TM014, NSC 100-2120-M-006-002, and NSC-100-2314-B-006-032-MY3.

Disclosure

The authors report no conflicts of interest in this work.

References

1. Liu P, Cheng H, Roberts TM, Zhao JJ. Targeting the phosphoinositide 3-kinase pathway in cancer. *Nat Rev Drug Discov*. 2009;8(8):627–644.
2. Markman B, Atzori F, Perez-Garcia J, Taberero J, Baselga J. Status of PI3K inhibition and biomarker development in cancer therapeutics. *Ann Oncol*. 2010;21(4):683–691.
3. Steelman LS, Stadelman KM, Chappell WH, et al. Akt as a therapeutic target in cancer. *Expert Opin Ther Targets*. 2008;12(9):1139–1165.
4. Hennessy BT, Smith DL, Ram PT, Lu Y, Mills GB. Exploiting the PI3K/AKT pathway for cancer drug discovery. *Nat Rev Drug Discov*. 2005;4(12):988–1004.
5. Yuan TL, Cantley LC. PI3K pathway alterations in cancer: variations on a theme. *Oncogene*. 2008;27(41):5497–5510.
6. Walker EH, Pacold ME, Perisic O, et al. Structural determinants of phosphoinositide 3-kinase inhibition by wortmannin, LY294002, quercetin, myricetin, and staurosporine. *Mol Cell*. 2000;6(4):909–919.
7. Hill MM, Hemmings BA. Inhibition of protein kinase B/Akt implications for cancer therapy. *Pharmacol Ther*. 2002;93(2–3):243–251.
8. Brognard J, Clark AS, Ni Y, Dennis PA. Akt/protein kinase B is constitutively active in non-small cell lung cancer cells and promotes cellular survival and resistance to chemotherapy and radiation. *Cancer Res*. 2001;61(10):3986–3997.
9. Krystal GW, Sulanke G, Litz J. Inhibition of phosphatidylinositol 3-kinase-Akt signaling blocks growth, promotes apoptosis, and enhances sensitivity of small cell lung cancer cells to chemotherapy. *Mol Cancer Ther*. 2002;1(11):913–922.
10. LoPiccolo J, Blumenthal GM, Bernstein WB, Dennis PA. Targeting the PI3K/Akt/mTOR pathway: effective combinations and clinical considerations. *Drug Resist Updat*. 2008;11(1–2):32–50.

11. Hu L, Hofmann J, Lu Y, Mills GB, Jaffe RB. Inhibition of phosphatidylinositol 3'-kinase increases efficacy of paclitaxel in in vitro and in vivo ovarian cancer models. *Cancer Res.* 2002;62(4):1087–1092.
12. Hu L, Zaloudek C, Mills GB, Gray J, Jaffe RB. In vivo and in vitro ovarian carcinoma growth inhibition by a phosphatidylinositol 3-kinase inhibitor (LY294002). *Clin Cancer Res.* 2000;6(3):880–886.
13. Jiang H, Fan D, Zhou G, Li X, Deng H. Phosphatidylinositol 3-kinase inhibitor(LY294002) induces apoptosis of human nasopharyngeal carcinoma in vitro and in vivo. *J Exp Clin Cancer Res.* 2010;29:34.
14. Marone R, Cmiljanovic V, Giese B, Wymann MP. Targeting phosphoinositide 3-kinase: moving towards therapy. *Biochim Biophys Acta.* 2008;1784(1):159–185.
15. Soppimath KS, Aminabhavi TM, Kulkarni AR, Rudzinski WE. Biodegradable polymeric nanoparticles as drug delivery devices. *J Control Release.* 2001;70(1–2):1–20.
16. West JL, Halas NJ. Applications of nanotechnology to biotechnology commentary. *Curr Opin Biotechnol.* 2000;11(2):215–217.
17. Hogemann D, Ntziachristos V, Josephson L, Weissleder R. High throughput magnetic resonance imaging for evaluating targeted nanoparticle probes. *Bioconjug Chem.* 2002;13(1):116–121.
18. Tkachenko AG, Xie H, Liu Y, et al. Cellular trajectories of peptide-modified gold particle complexes: comparison of nuclear localization signals and peptide transduction domains. *Bioconjug Chem.* 2004;15(3):482–490.
19. Parveen S, Sahoo SK. Polymeric nanoparticles for cancer therapy. *J Drug Target.* 2008;16(2):108–123.
20. Di Toro R, Betti V, Spampinato S. Biocompatibility and integrin-mediated adhesion of human osteoblasts to poly(DL-lactide-co-glycolide) copolymers. *Eur J Pharm Sci.* 2004;21(2–3):161–169.
21. Danhier F, Ansorena E, Silva JM, Coco R, Le Breton A, Preat V. PLGA-based nanoparticles: An overview of biomedical applications. *J Control Release.* 2012;161(2):505–522.
22. Esmaili F, Ghahremani MH, Esmaili B, Khoshayand MR, Atyabi F, Dinarvand R. PLGA nanoparticles of different surface properties: preparation and evaluation of their body distribution. *Int J Pharm.* 2008;349(1–2):249–255.
23. Mundargi RC, Babu VR, Rangaswamy V, Patel P, Aminabhavi TM. Nano/micro technologies for delivering macromolecular therapeutics using poly(D,L-lactide-co-glycolide) and its derivatives. *J Control Release.* 2008;125(3):193–209.
24. Harfouche R, Basu S, Soni S, Hentschel DM, Mashelkar RA, Sengupta S. Nanoparticle-mediated targeting of phosphatidylinositol-3-kinase signaling inhibits angiogenesis. *Angiogenesis.* 2009;12(4):325–338.
25. Sahoo SK, Panyam J, Prabha S, Labhasetwar V. Residual polyvinyl alcohol associated with poly (D,L-lactide-co-glycolide) nanoparticles affects their physical properties and cellular uptake. *J Control Release.* 2002;82(1):105–114.
26. Cheng FY, Wang SP, Su CH, et al. Stabilizer-free poly(lactide-co-glycolide) nanoparticles for multimodal biomedical probes. *Biomaterials.* 2008;29(13):2104–2112.
27. Kuo WS, Ku YC, Sei, HT, Cheng FY, Yeh CS. Paclitaxel-loaded stabilizer-free poly(D,L-lactide-co-glycolide) nanoparticles conjugated with quantum dots for reversion of anti-cancer drug resistance and cancer cellular imaging. *Chin Chem Soc.* 2009;56(5):923–934.
28. Yeh HH, Lai WW, Chen HH, Liu HS, Su WC. Autocrine IL-6-induced Stat3 activation contributes to the pathogenesis of lung adenocarcinoma and malignant pleural effusion. *Oncogene.* 2006;25(31):4300–4309.
29. Schafer ZT, Kornbluth S. The apoptosome: physiological, developmental, and pathological modes of regulation. *Dev Cell.* 2006;10(5):549–561.
30. Oyadomari S, Mori M. Roles of CHOP/GADD153 in endoplasmic reticulum stress. *Cell Death Differ.* 2004;11(4):381–389.
31. Lee H, Park MT, Choi BH, et al. Endoplasmic reticulum stress-induced JNK activation is a critical event leading to mitochondria-mediated cell death caused by beta-lapachone treatment. *PLoS One.* 2011;6(6):e21533.
32. Kroemer G, Mariño G, Levine B. Autophagy and the integrated stress response. *Mol Cell.* 2010;40(2):280–293.
33. Sinha R, Kim GJ, Nie S, Shin DM. Nanotechnology in cancer therapeutics: bioconjugated nanoparticles for drug delivery. *Mol Cancer Ther.* 2006;5(8):1909–1917.
34. Moghimi SM, Hunter AC, Murray JC. Nanomedicine: current status and future prospects. *FASEB J.* 2005;19(3):311–330.
35. Torche AM, Le Corre P, Albina E, Jestin A, Le Verge R. PLGA microspheres phagocytosis by pig alveolar macrophages: influence of poly(vinyl alcohol) concentration, nature of loaded-protein and copolymer nature. *J Drug Target.* 2000;7(5):343–354.
36. Prabha S, Labhasetwar V. Critical determinants in PLGA/PLA nanoparticle-mediated gene expression. *Pharm Res.* 2004;21(2):354–364.
37. Brognard J, Clark AS, Ni Y, Dennis PA. Akt/protein kinase B is constitutively active in non-small cell lung cancer cells and promotes cellular survival and resistance to chemotherapy and radiation. *Cancer Res.* 2001;61(10):3986–3997.
38. Paulo CS, Pires das Neves R, Ferreira LS. Nanoparticles for intracellular-targeted drug delivery. *Nanotechnology.* 2011;22(49):494002.

Supplementary materials

Materials and methods

Flow cytometric analysis

Asynchronous cultures were set for experiments (2×10^5 cells in 6-well plates). Individual wells were treated with free LY or SF-LY NPs for 24 hours. Cells were stained according to the manufacturer's instructions with Annexin V-fluorescein isothiocyanate and propidium iodide staining assay kit (Life Technologies) and measured by flow cytometry (BD FACS-Calibur System; BD Biosciences, San Jose, CA, USA).

DAPI staining for chromosome condensation

Chromosome condensation due to free LY and SF-LY NPs in cell lines was observed by DAPI staining. DAPI solution was used to stain the exposed cells in chamber slides, which were incubated for 10 minutes in the dark at 37°C. Images of the nucleus were captured using a fluorescence microscope (Nikon Corporation, Tokyo, Japan) at an excitation wavelength of 330 nm and an emission wavelength of 420 nm.

MTT cytotoxicity assay

Cells were seeded (5×10^3 per well) in a 96-well culture plate and incubated overnight at 37°C in humidified air containing 5% CO₂. Concentration–effect and time-course studies were performed in the presence of free LY, SF NPs, and SF-LY NPs. After the required incubation periods, 20 µL of MTT reagent stock solution (5 mg/mL in PBS) was added to each well and incubated for 4 hours at 37°C. Plates were centrifuged at 1200 rpm for 5 minutes. After discarding the supernatant, DMSO (200 µL) was added into each well and incubated for 5 minutes. Supernatants were transferred into a new ELISA plate and absorbance was measured at

490 nm with an ELISA reader (Varioskan; Thermo Fisher Scientific).

Intracellular localization by confocal laser microscopy

Viable cells (1×10^5) were plated onto 3.5 cm dishes with 3 mL of culture medium. After overnight incubation, cells were treated with free Nile red or PLGA NPs loaded with Nile red (PVA-Nile red NPs) for 3 hours of incubation and stained with ER tracker™ Green dye according to the manufacturer's protocol (Molecular Probes®, Life Technologies) and DAPI. After replacement of original medium with particle-free, fresh medium, cells were immediately imaged with a scanning confocal microscope (Fluoview® FV-1000; Olympus Corporation) with settings to detect fluorophores by A laser (excitation 405, 488, or 546 nm).

Western blot analysis

Cells were lysed on ice for 30 minutes with whole-cell extract lysis buffer (50 mM Tris-HCl, pH 7.2–7.8; 1% NP-40; 2 mM EDTA; 100 mM NaCl; 0.1% SDS supplemented with protease inhibitor cocktail; Roche Applied Sciences). Lysates were collected by centrifugation at 14,000 rpm for 10 minutes, and protein concentration was determined using the Bradford assay (Bio-Rad). Protein extracts (20–50 µg) were boiled for 5 minutes in sample buffer before separation by SDS-PAGE. The proteins were transferred to PVDF membranes (Millipore) at 400 mA for 1.5 hours using an electroblotter (Amersham Pharmacia Biotech Inc). Membranes were blocked with TBST containing 5% nonfat milk for 1 hour at room temperature and incubated overnight at 4°C with LC3 or CHOP antibodies. Proteins were detected with horseradish peroxidase-conjugated secondary antibodies using an ECL kit (Amersham) according to the manufacturer's instructions.

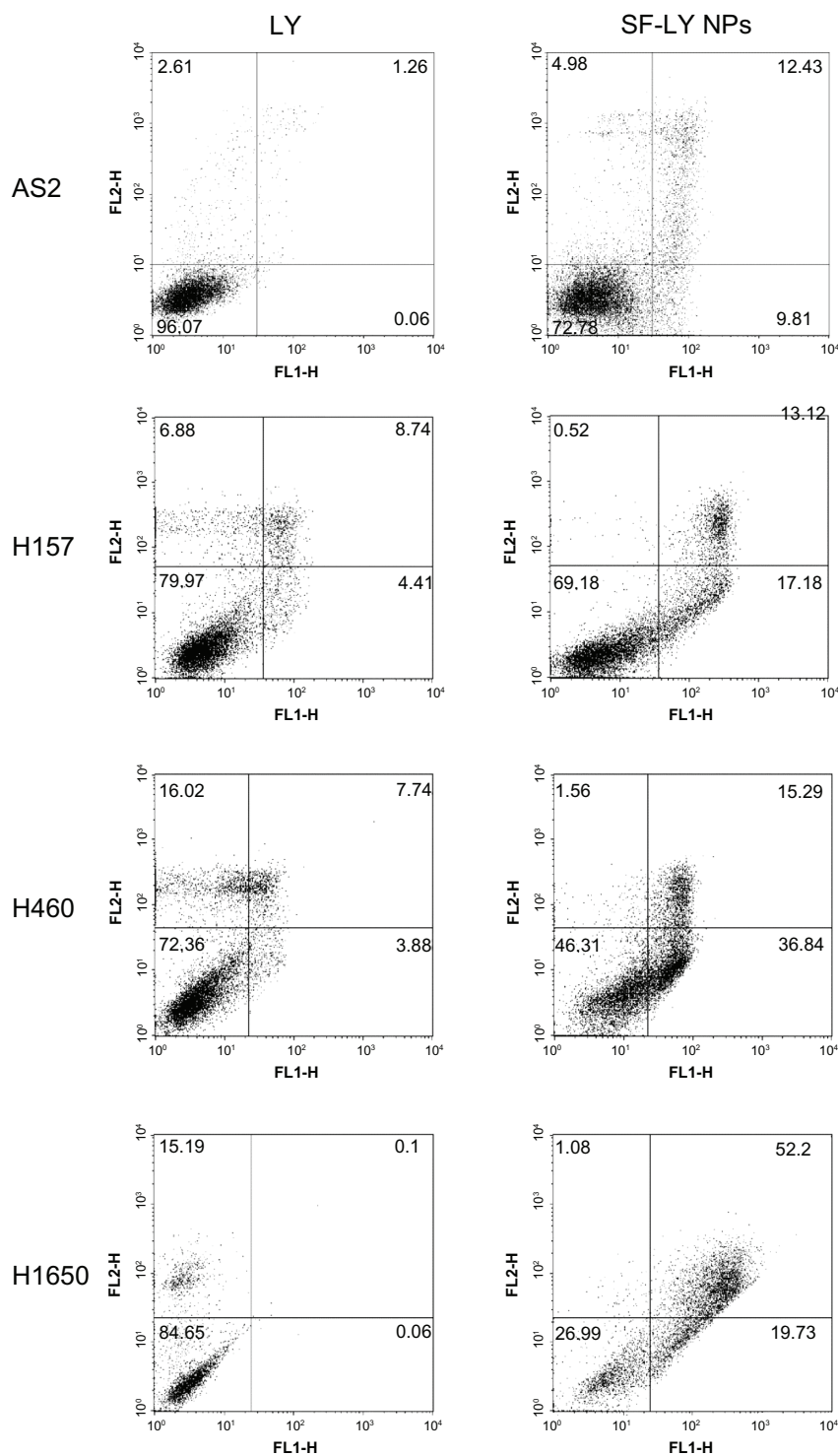


Figure S1 The level of apoptosis after exposure to free LY or SF-LY NPs.

Notes: The graphs present flow analysis of four cell lines treated with free LY or SF-LY NPs for 24 hours. The scatter plot of FL1-H (X-scale) versus FL2-H (Y-scale) indicates annexin V staining and propidium iodide staining.

Abbreviations: LY, LY294002; NPs, nanoparticles; SF-LY NPs, surfactant-free NPs loaded with LY.

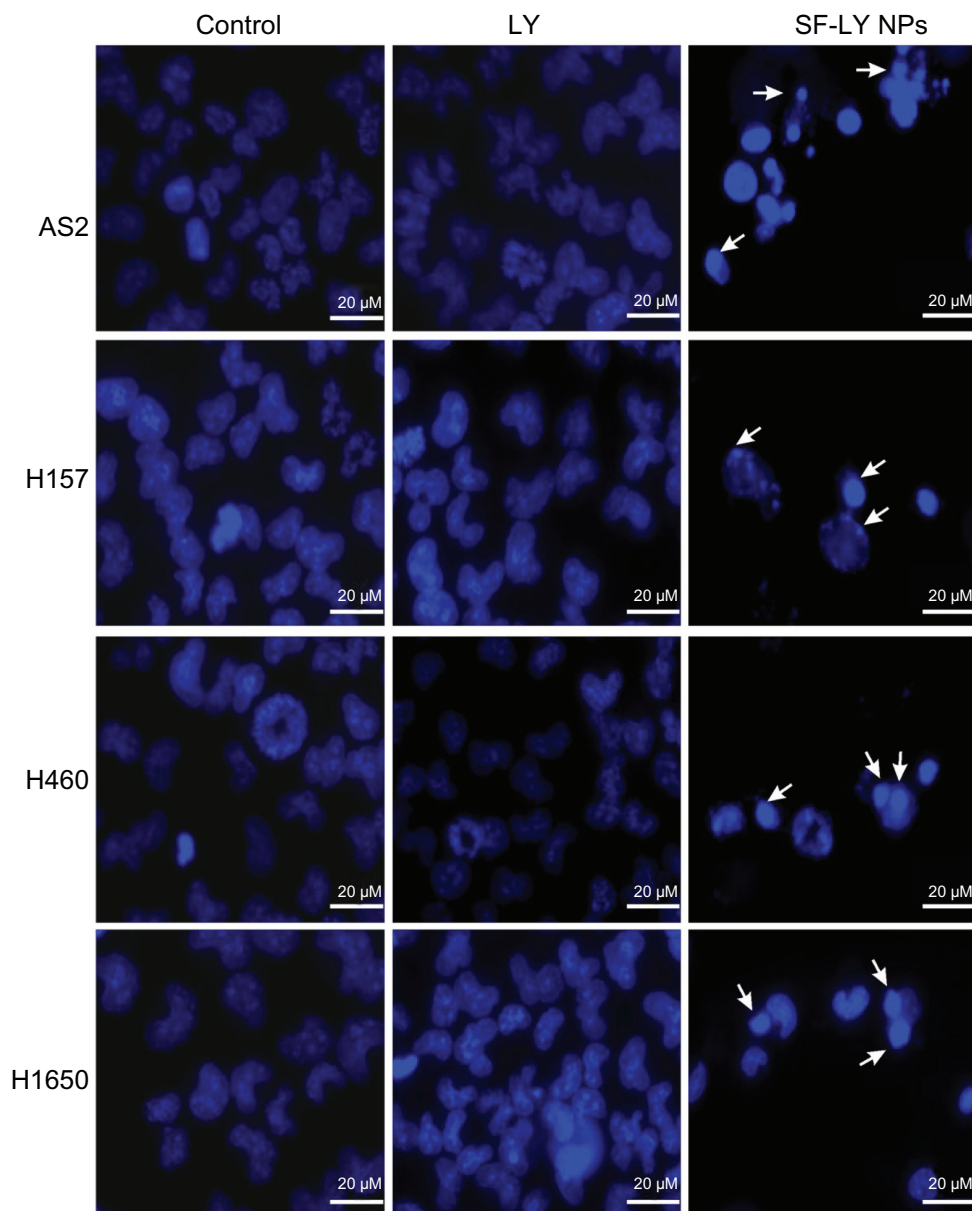


Figure S2 The level of chromatin condensation after exposure to free LY or SF-LY NPs.

Notes: The graphs show chromatin stained by DAPI after exposure to LY and SF-LY NPs at a concentration equivalent to that of LY for 24 hours in the four cell lines. The arrow indicates chromatin condensation.

Abbreviations: DAPI, 4',6-diamidino-2-phenylindole; LY, LY294002; NPs, nanoparticles; SF-LY NPs, surfactant-free NPs loaded with LY.

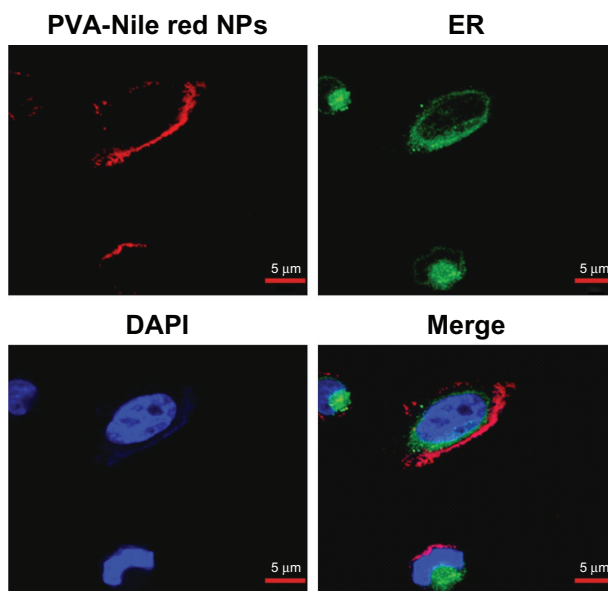


Figure S3 Intracellular localization of PVA NPs in cells.

Notes: Confocal microscopic analysis of PVA-Nile red NPs. The cells were incubated with PVA-Nile red NPs for 3 hours at 37°C, stained with ER tracker and DAPI, extensively washed, and imaged for living cells under a confocal microscope.

Abbreviations: DAPI, 4',6-diamidino-2-phenylindole; ER, endoplasmic reticulum; NPs, nanoparticles; PVA, polyvinyl alcohol; PVA-Nile red NPs, PVA NPs loaded with Nile red.

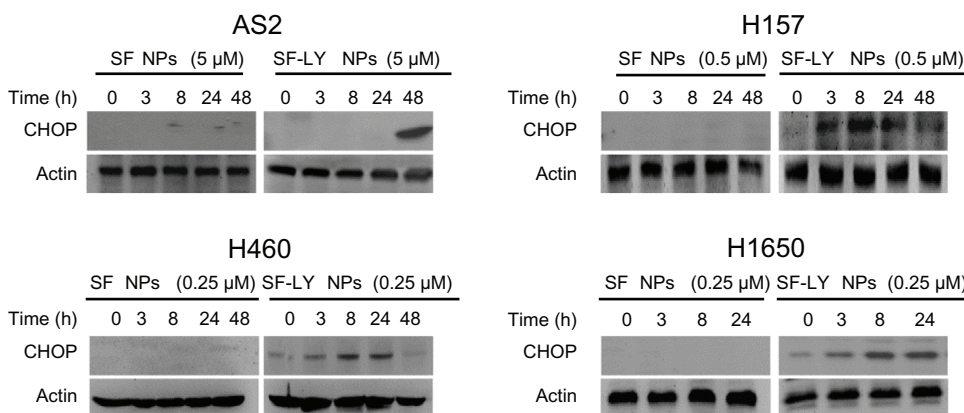


Figure S4 The level of CHOP after exposure to SF NPs or SF-LY NPs.

Notes: Western blots showing levels of CHOP in the four cell lines following treatment with SF NPs or SF-LY NPs for a time-course study.

Abbreviations: LY, LY294002; NPs, nanoparticles; SF NPs, surfactant-free NPs; SF-LY NPs, surfactant-free NPs loaded with LY; h, hours.

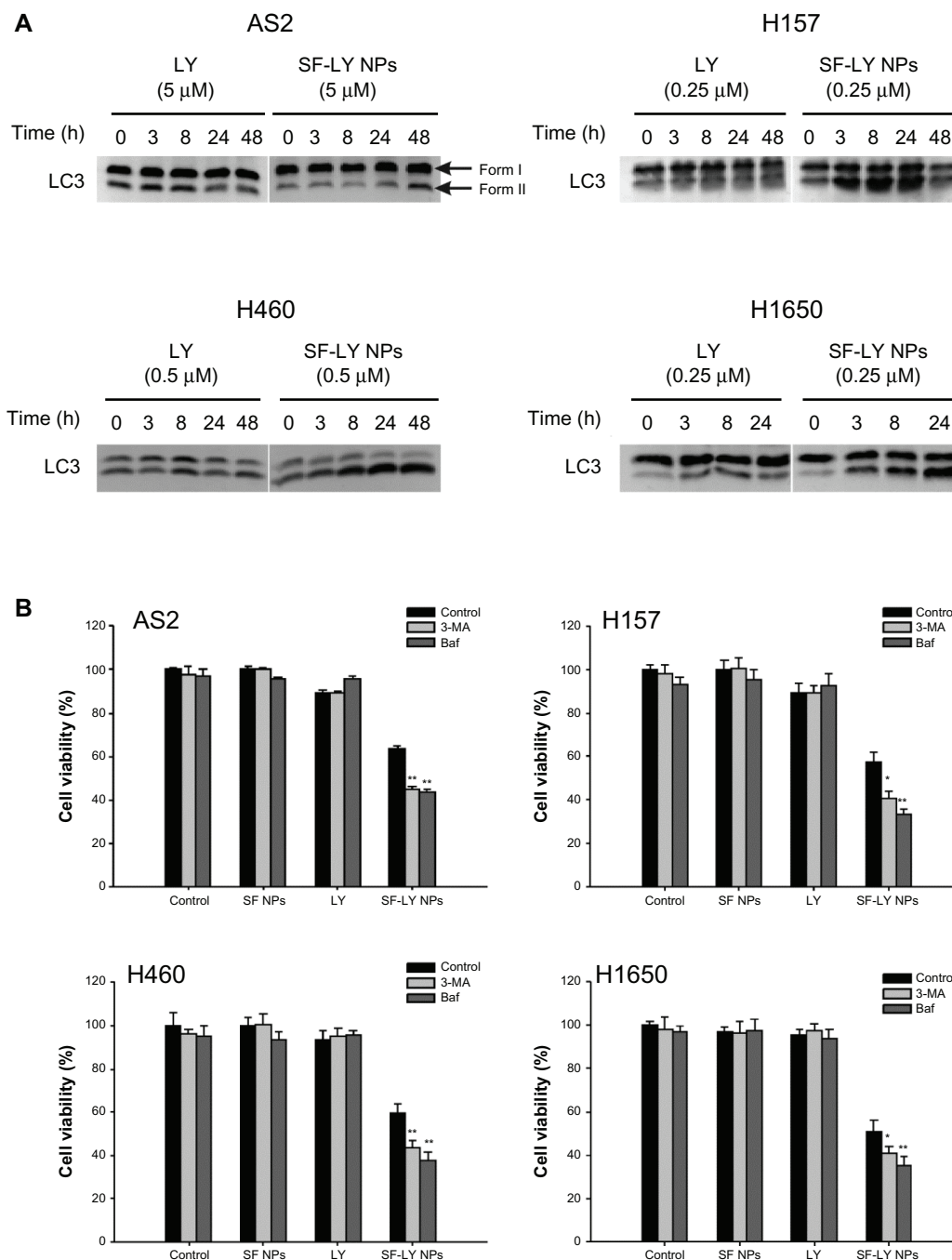


Figure S5 The regulation of autophagy after treatment with free LY or SF-LY NPs.

Notes: (A) Western blots showing levels of LC3 in four cell lines following treatment with LY or SF-LY NPs for a time-course study. (B) The analysis of cytotoxicity by MTT assay after treatment with 3-MA (5 mM) or bafilomycin A1 (1 nM). Each experiment was repeated three times. Data are mean \pm SEM. * $P < 0.05$; ** $P < 0.005$.

Abbreviations: 3-MA, 3-methyladenine; baf, bafilomycin; A1LY, LY294002; MTT, 3-[4,5-dimethylthiazol-2-yl]-2, 5-diphenyltetrazolium bromide; NPs, nanoparticles; SEM, standard error of the mean; SF-LY NPs, surfactant-free NPs loaded with LY; h, hours.